Dalton Transactions

Accepted Manuscript

ROYAL SOCIETY OF CHEMISTRY

www.rsc.org/dalton

Dalton Transactions

RSC Publishing

ARTICLE

Heteroleptic Cationic Iridium(III) Complexes Bearing Naphthalimidyl Substituents: Synthesis, Photophysics and Reverse Saturable Absorption

Cite this: DOI: 10.1039/x0xx00000x

Received 00th July 2014,
Accepted 00th xxx 2014

DOI: 10.1039/x0xx00000x

www.rsc.org/

Chengkui Pei,[a] Peng Cui,[a,b] Christopher McCleese,[c] Svetlana Kilina,[a,*] Clemens Burda,[c,*] Wenfang Sun[a,*]

Three heteroleptic cationic iridium(III) complexes containing cyclometalating 2-[3-(7-naphthalimidylfluoren-2′-yl)phenyl]pyridine ligand and different diimine (N^N) ligands (N^N = 2,2'-bipyridine (bpy, **Ir-1**), 1,10-phenanthroline (phen, **Ir-2**), and 5,5'-bis[7-(benzothiazol-2'-yl)fluoren-2'-yl]-2,2'-bipyridine (BTF-bpy, **Ir-3**)) were synthesized and characterized. The photophysics of these complexes was systematically investigated via spectroscopic methods and by time-dependent density functional theory (TDDFT). All complexes possess a very weak charge-transfer tail at ca. 450 – 570 nm; and two intense absorption bands in the region of 290 – 350 nm and 350 – 450 nm, respectively. The emission of **Ir-1** – **Ir-3** in CH_2Cl_2 emanates predominantly from the C^N ligand-localized $^3\pi,\pi^*$ state. These emitting excited states also give rise to broadband triplet excited-state absorption in the visible to the near-IR region (*i.e.* 420 – 800 nm for **Ir-1** and **Ir-2**, and 460 – 800 nm for **Ir-3**). The kinetics of fs TA reveals that the lowest singlet excited-state lifetimes of these complexes vary from 1.43 ps to 142 ps. The stronger excited-state absorption of **Ir-1** – **Ir-3** compared to their respective ground-state absorption in the visible spectral range leads to strong reverse saturable absorption (RSA) at 532 nm for ns laser pulses. The trend of transmission signal decrease follows **Ir-2** > **Ir-3** > **Ir-1**. Extending the π-conjugation of the N^N ligand increases the strength of RSA. In addition, the naphthalimidyl (NI) substitution at the C^N ligand dramatically increases the triplet excited-state lifetimes and broadens the triplet excited-state absorption to the NIR region compared to the respective Ir(III) complexes with benzothiazolyl substituent on the C^N ligand.

Introduction

Octahedral d^6 Ru(II) and Os(II) complexes have been well studied for their photoluminescence properties.[1] Diimine ligands (N^N), such as 2,2'-bipyridine (bpy) and 1,10-phenanthroline (phen), have been used for modulating the luminescence properties of the Ru(II) and Os(II) complexes in many studies.[2] Meanwhile, tris-chelated rhodium(III) and iridium(III) complexes with diimine and / or cyclometalating bidentate ligands have also attracted much attention in the last decade.[3,4] In contrast to the Rh(III) complexes that emit only at low temperature, the Ir(III) complexes demonstrate intensive phosphorescence at room temperature.[5] In addition, a strong spin-orbit coupling admixes the singlet and triplet excited states, which increases the phosphorescence efficiency and broadens the light absorption to the longer visible and the near-IR region. The latter is due to direct absorption from the singlet ground state to the triplet excited state in iridium complexes.[6-8] Therefore, the Ir(III) complexes have been widely investigated as photosensitizers for catalytic photoinduced hydrogen production[9,10] and solar cell applications,[11-13] and as emitters for electroluminescence device applications.[14,15] Moreover, Ir(III) complexes are considered as promising photocatalysts, which facilitate water oxidation and CO_2 reduction reactions due to their broad visible-light absorption and long-lived triplet excited states.[16-19]

It is well known that the emission energy and lifetime of the heteroleptic Ir(III) complexes bearing bipyridyl (bpy, N^N ligand) and cyclometalating 2-phenylpyridine (ppy, C^N ligand) ligands could be adjusted by the electron-withdrawing or electron-donating substituents on the bpy or ppy ligands.[20-24] Also, an extension of the π-conjugation of the N^N or C^N ligands could efficiently tune the emission energy and lifetime of the Ir(III) complexes as well.[25-34] Our group has studied several series of Ir(III) complexes with a benzothiazolylfluorenyl (BTF) group attached on the N^N or C^N ligands. We found that extending the π-conjugation of the N^N ligand via attaching the BTF groups prolonged the lifetime of the lowest triplet excited state, while incorporating the BTF groups on the C^N ligands reduced the triplet lifetime.[35-37]

The reported work on the heteroleptic cationic Ir(III) complexes is intriguing. However, studies on using the Ir(III) complexes as nonlinear optical materials has been quite limited. To date, only handful reports are found in the literature on investigating the reverse saturable absorption (RSA, *i.e.* the absorptivity of the material increases with the increased incident energy) of the Ir(III) complexes.[26,35-37] It is well known that RSA has important

applications in optical switching, optical rectification, laser pulse shaping and compression, etc. An ideal reverse saturable absorber is required to possess a large ratio of the excited-state absorption cross section with respect to that of the ground-state absorption in the visible to the near-IR region, and the excited-state lifetime should be longer than the laser pulse width. For RSA of ns laser pulses, high triplet quantum yield is another desirable feature. Developing organic or inorganic materials that can meet all these requirements have been keeping as a challenging for the nonlinear optical materials field. To realize this goal, understanding the structure-property correlation is the key.

Our group previously discovered that the different substituents on the 2-(7'-R-fluoren-2'-yl)pyridine ligands influenced the RSA of the Ir(III) complexes significantly.[36] It has also been revealed that the Pt(II) bipyridyl complexes bearing the naphthalimidyl (NI) group on the acetylide ligands possessed an extremely long-lived lowest triplet excited state and broadband excited-state absorption,[38-40] which led to very strong RSA by the Pt(II) complexes at 532 nm.[40] Inspired by these results, we intend to modify the C^N ligand used in our reported heteroleptic cationic Ir(III) complexes[35,37] by replacing the benzothiazolyl (BTZ) group on the fluorenyl motif with the NI group. Such a modification is expected to further improve the RSA of the Ir(III) complexes, since NI group has been demonstrated to dramatically increase the lifetime of the lowest triplet excited state and broaden the excited-state absorption to the near-IR region in the Pt(II) acetylide complexes[38-40] – both of them are important prerequisites for enhanced RSA. As such, we synthesized three new cationic Ir(III) complexes (**Ir-1** - **Ir-3** in Chart 1) with a NI substituent on the 7-position of the fluorenyl group in the C^N ligands. 2,2'-Bipyridine (bpy), 1,10-phenanthroline (phen) and 5,5'-di(7-benzothiazolylfluoren-2-yl)-2,2'-bipyridine (BTF-bpy)[41] were selected as the N^N ligand in these complexes, respectively. Our group previously found that Ir(III) complexes containing the substituted phenanthroline ligand (such as the complexes **2** and **5** in Ref. 37 with τ_T of 11.3 μs and 290 ns in toluene, respectively) exhibited longer triplet lifetime than the corresponding complexes with the substituted bipyridine ligand (such as the complexes **2** and **3** in Ref 35 with τ_T of 8.35 μs and 200 ns in toluene, respectively). Therefore, we anticipate that replacing the bpy ligand in **Ir-1** by the phen ligand in **Ir-2** could increase the triplet lifetime of **Ir-2**. Using the BTF-bpy ligand in **Ir-3** would allow us to further demonstrate the effect of extended π-conjugation in the N^N ligand. The photophysical properties and reverse saturable absorption of these complexes were systematically investigated in order to reveal the effect of the NI group on the C^N ligands. To illustrate the role of the NI groups and π-conjugation of the C^N or N^N ligands in the photoexcitation and emission of these complexes, we also performed density functional theory (DFT) and linear-response time dependent DFT (TDDFT) calculations. Calculated results complement our experimental data by providing additional insights into the structural characteristics and the charge transfer character of excited states in **Ir-1** - **Ir-3**.

Experimental section

Synthesis and characterization

All reagents and solvents were purchased from commercial sources and used as is unless otherwise mentioned. ^{1}H NMR spectra were recorded on a Varian Oxford-400 or Varian Oxford-500 spectrometer in $CDCl_3$ with tetramethylsilane (TMS) as internal standard. High resolution mass (HRMS) analyses were performed on a Bruker BioTof III mass spectrometer. Elemental analyses were conducted by NuMega Resonance Laboratories, Inc. in San Diego, CA.

The synthetic route for **Ir-1** – **Ir-3** is illustrated in Scheme 1. Precursors **1**,[42,43] **3**,[38-40] and **5**[44] were synthesized following the literature procedures. The synthesis of ligand **8** was reported by our group previously.[41] The synthetic procedures and characterization data for compounds **2**, **4**, **6**, **7** and the complexes **Ir-1** – **Ir-3** are reported in the following.

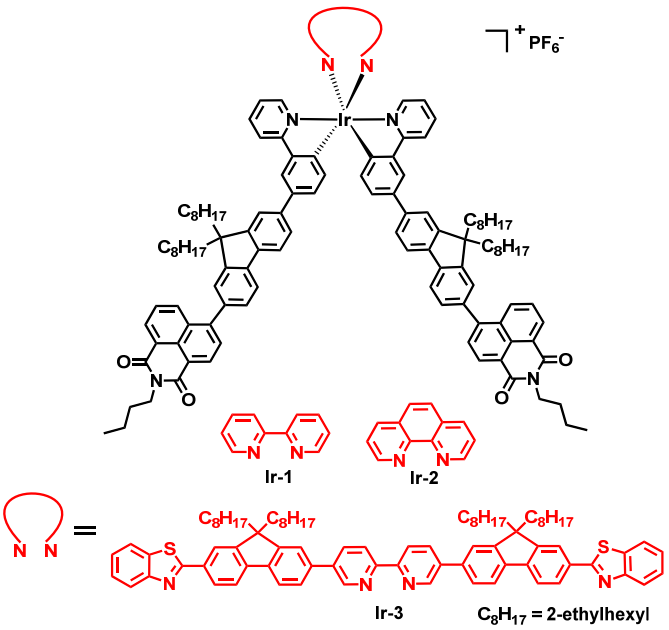

Chart 1 Structures of the Ir(III) complexes **Ir-1** - **Ir-3**.

2. Compound **1** (5.00 g, 9.16 mmol) was dissolved in 20 mL of absolute THF. The solution was degassed with argon and cooled down to -78 ^{o}C. Then 10 mL of ^{n}BuLi hexane solution (2.5 M, 25 mmol) was added dropwise at -78 ^{o}C under argon atmosphere. The mixture was stirred at this temperature for 1.5 h, and 2-isopropoxy-4,4,5,5-tetramethyl-1,3,2-dioxaborolane (ITDB) (8 mL, 22.9 mmol) was added in about 15 min. The reaction mixture was allowed to gradually warm up to r.t. and stirred for overnight. 2 M HCl was added and stirred for 0.5 h to quench the reaction. The organic layer was separated and the aqueous layer was extracted with CH_2Cl_2 (25 mL × 2). The organic phase was combined and dried over $MgSO_4$. The solvent was then removed under reduced pressure, and the residue was purified by elution through column chromatography (silica gel, hexane/ethyl acetate = 50/1 (v/v) was used as the eluent) to obtain product **2** as yellow oil (3.2 g, yield: 54%). ^{1}H NMR ($CDCl_3$, 400 MHz) δ 0.40-0.52 (m, 8H), 0.71-0.95 (m, 22H), 1.42 (s, 24H), 1.96-2.19 (m, 4H), 7.60-7.68 (m, 2H), 7.69-7.78 (m, 2H), 7.79-7.85 (m, 2H).

4. Compounds **2** (320 mg, 0.5 mmol), **3** (96 mg, 0.3 mmol), $Pd(PPh_3)_4$ (35 mg, 0.03 mmol), and 2 M K_2CO_3 aqueous solution (2 mL) were added in 10 mL toluene. The mixture was heated to reflux under argon for 24 h. After cooling down to room temperature, the

solution was concentrated in vacuum, and then extracted with CH_2Cl_2. The CH_2Cl_2 layer was washed with brine and dried over $MgSO_4$. The solvent was removed and the crude product was purified by column chromatography (SiO_2, hexane/ethyl acetate = 50/1 (v/v)) to get product **4** as yellow oil (110 mg, yield: 46%). ^{1}H NMR ($CDCl_3$, 400 MHz) δ 0.46-0.75 (m, 12H), 0.76-0.98 (m, 21H), 1.42 (s, 12H), 1.46-1.50 (m, 2H), 1.68-1.75 (m, 2H), 1.90-2.12 (m, 4H), 4.22 (t, J = 7.2 Hz, 2H), 7.40-7.49 (m, 2H), 7.60-7.68 (m, 2H), 7.75-7.78 (m, 1H), 7.80-7.85 (m, 3H), 8.20-8.30 (m, 1H), 8.60-8.70 (m, 2H).

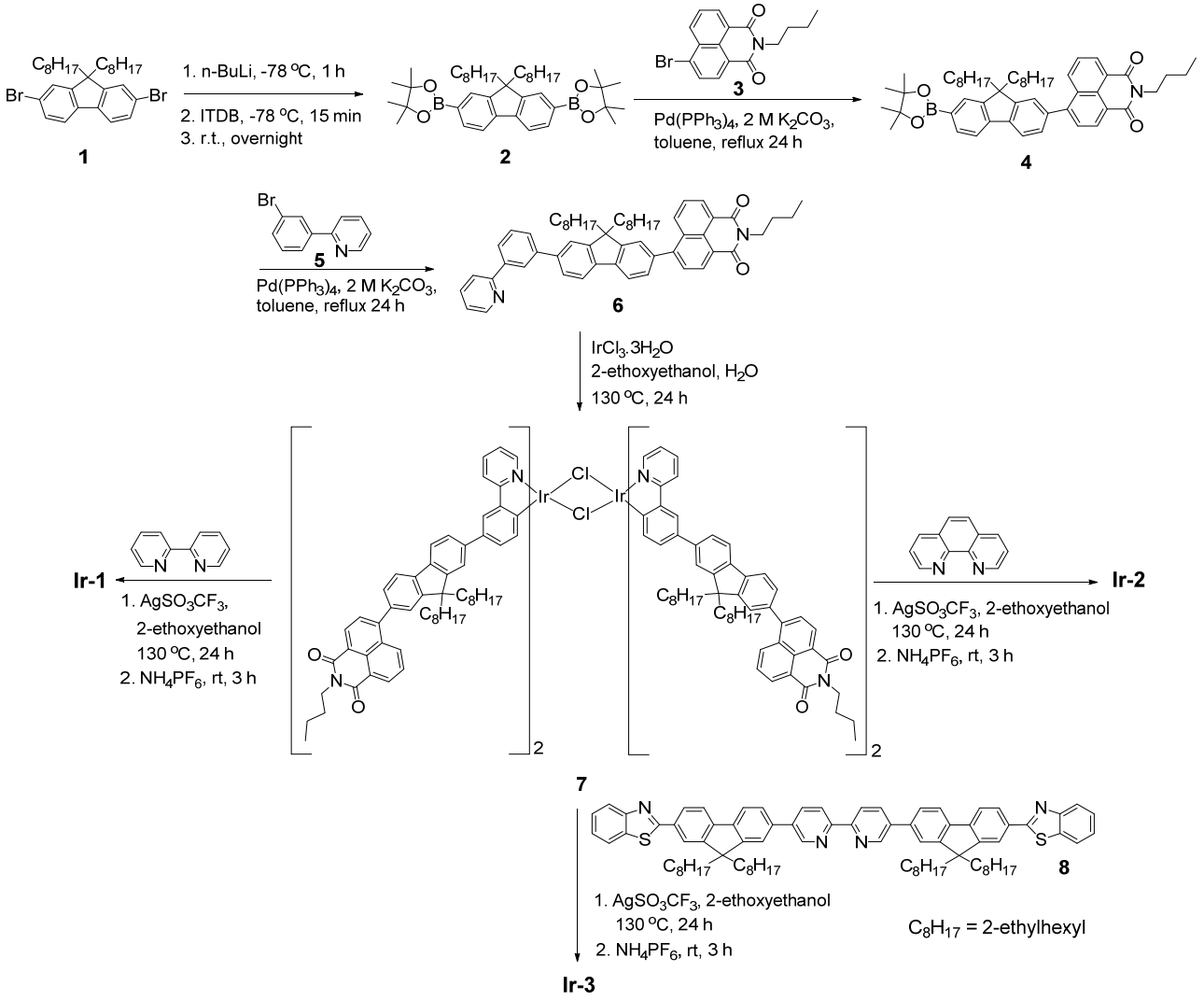

Scheme 1 Synthetic route for **Ir-1** - **Ir-3**.

6. Compounds **4** (110 mg, 0.14 mmol), **5** (46 mg, 0.20 mmol), $Pd(PPh_3)_4$ (30 mg, 0.02 mmol), and 2 M K_2CO_3 aqueous solution (1 mL) were added in 10 mL toluene. The mixture was heated to reflux under argon for 24 h. After cooling down to room temperature, the solution was concentrated in vacuum, and then extracted with CH_2Cl_2. The CH_2Cl_2 layer was washed with brine and dried over $MgSO_4$. The solvent was then removed and the crude product was purified by column chromatography (SiO_2, hexane/EA = 50/1 (v/v)) to obtain product **6** as yellow oil (60 mg, yield: 59%). ^{1}H NMR ($CDCl_3$, 400 MHz) δ 0.57-0.63 (m, 12H), 0.81-0.99 (m, 21H), 1.44-1.50 (m, 2H), 1.73-1.77 (m, 2H), 2.04-2.16 (m, 4H), 4.22 (t, J = 7.2 Hz, 2H), 7.24-7.27 (m, 1H), 7.44-7.50 (m, 2H), 7.55-7.59 (m, 1H), 7.65-7.70 (m, 5H), 7.77-7.79 (m, 2H), 7.84 (d, J = 8.4 Hz, 1H), 7.88 (d, J = 7.6 Hz, 1H), 7.97 (d, J = 7.6 Hz, 1H), 8.25-8.30 (m, 2H), 8.63-8.67 (m, 2H), 8.73-8.74 (m, 1H). HRMS (ESI) calcd. for $C_{56}H_{63}N_2O_2$ (M+H): 795.4884, Found: 795.4888. Anal calcd (%) for $C_{56}H_{62}N_2O_2 \cdot CH_2Cl_2 \cdot 2C_6H_{14}$: C, 78.75; H, 8.81; N, 2.66. Found: C, 78.38; H, 8.61; N, 3.06.

7. Ligand **6** (400 mg, 0.50 mmol) and $IrCl_3 \cdot 3H_2O$ (82 mg, 0.25 mmol) were dissolved in a mixture of 2-ethoxyethanol (10 mL) and

water (3 mL), and the mixture was heated at 130 °C for 24 h. After that, the mixture was cooled down to r.t. and the precipitate was collected by filtration as yellow solid. The yellow solid was washed with EtOH (20 mL) and acetone (20 mL) first, and then dissolved in CH_2Cl_2 (25 mL). The undissolved solid was removed by filtration and methanol (30 mL) was added to the filtrate to precipitate orange solid 200 mg as compound **7**.

Ir-1. The mixture of **7** (89 mg, 0.025 mmol), bpy (8 mg, 0.05 mmol) and $AgSO_3CF_3$ (12.5 mg, 0.05 mmol) in 2-ethoxyethanol (5 mL) and water (3 mL) was heated at 130 °C for 24 h. Then the mixture was cooled down to r.t., and NH_4PF_6 (16.3 mg, 0.10 mmol) was added and stirred at r.t. for 3 h. After the reaction, the solvent was removed and the residue was purified by column chromatography (CH_2Cl_2/ethyl acetate = 50/1 (v/v)) to yield yellow solid 50 mg (yield: 50% for two steps from ligand **6**). ^{1}H NMR ($CDCl_3$, 400 MHz) δ 0.57-0.63 (m, 24H), 0.81-0.99 (m, 42H), 1.44-1.50 (m, 4H), 1.73-1.77 (m, 4H), 2.04-2.16 (m, 8H), 4.22 (t, J = 7.2 Hz, 4H), 6.45-6.55 (m, 2H), 7.09-7.13 (m, 2H), 7.24-7.27 (m, 2H), 7.44-7.50 (m, 6H), 7.65-7.70 (m, 10H), 7.79-7.85 (m, 6H), 7.87-7.90 (m, 2H), 8.00-8.10 (m, 4H), 8.17-8.28 (m, 4H), 8.61-8.69 (m, 6H). HRMS (ESI) calcd. for $C_{122}H_{130}IrN_6O_4$ (M-PF_6): 1936.9831, Found: 1936.9817. Anal calcd (%) for $C_{122}H_{130}IrN_6O_4PF_6{\cdot}1.5CH_2Cl_2$: C, 67.15; H, 6.07; N, 3.80. Found: C, 67.09; H, 5.65; N, 3.70.

Ir-2. The mixture of **7** (72 mg, 0.02 mmol), 1,10-phenanthroline (7.2 mg, 0.04 mmol) and $AgSO_3CF_3$ (10 mg, 0.04 mmol) in 2-ethoxyethanol (3 mL) and water (2 mL) was heated to 130 °C for 24 h. Then the reaction mixture was cooled down to r.t., and NH_4PF_6 (12.5 mg, 0.04 mmol) was added and stirred at r.t. for 3 h. The solvent was removed and the residue was purified by column chromatography (CH_2Cl_2/ethyl acetate = 50/1 (v/v)) to get yellow solid 43 mg (yield: 47% for two steps from ligand **6**). ^{1}H NMR ($CDCl_3$, 400 MHz) δ 0.53-0.70 (m, 28H), 0.71-1.02 (m, 38H), 1.43-1.48 (m, 4H), 1.72-1.76 (m, 4H), 1.96-2.19 (m, 8H), 4.21 (t, J = 7.2 Hz, 4H), 6.57-6.59 (m, 2H), 7.00 (t, J = 6.8 Hz, 2H), 7.32 (d, J = 7.2 Hz, 2H), 7.43-7.52 (m, 6H), 7.62-7.70 (m, 8H), 7.79-7.87 (m, 8H), 8.00-8.06 (m, 4H), 8.23-8.26 (m, 4H), 8.34-8.38 (m, 2H), 8.62-8.70 (m, 6H). HRMS (ESI) calcd. for $C_{124}H_{130}IrN_6O_4$ (M-PF_6): 1960.9817, Found: 1960.9794. Anal calcd (%) for $C_{124}H_{130}IrN_6O_4PF_6{\cdot}2H_2O$: C, 69.54; H, 6.31; N, 3.92. Found: C, 69.21; H, 5.92; N, 3.80.

Ir-3. Complex **7** (36 mg, 0.01 mmol), ligand **8** (24 mg, 0.02 mmol) and $AgSO_3CF_3$ (10 mg, 0.04 mmol) in a mixture of 2-ethoxyethanol (3 mL) and water (2 mL) was heated to 130 °C for 24 h. Then the reaction mixture was cooled down to r.t., and NH_4PF_6 (12.5 mg, 0.04 mmol) was added and stirred at r.t. for 3 h. The solvent was removed and the residue was purified by column chromatography (CH_2Cl_2/ethyl acetate = 50/1 (v/v)) to get yellow solid 21 mg (yield: 30% for two steps from ligand **6**). ^{1}H NMR ($CDCl_3$, 400 MHz) δ 0.42-0.98 (m, 126H), 1.44-1.49 (m, 4H), 1.73-1.78 (m, 4H), 1.86-2.19 (m, 16H), 4.22 (t, J = 7.6 Hz, 4H), 6.60-6.61 (m, 2H), 7.11-7.19 (m, 2H), 7.37 (t, J = 7.2 Hz, 6H), 7.41-7.58 (m, 8H), 7.60-7.80 (m, 14H), 7.81-7.89 (m, 8H), 8.10-8.18 (m, 10H), 8.25-8.31 (m, 2H), 8.42-8.56 (m, 4H), 8.65 (t, J = 7.6 Hz, 4H), 8.84-8.92 (m, 2H). HRMS (ESI) calcd. for $C_{194}H_{216}IrN_8O_4S_2$ (M-PF_6): 2979.6053, Found: 2979.6122. Anal calcd (%) for $C_{194}H_{216}IrN_8O_4S_2PF_6{\cdot}4CHCl_3$: C, 66.01; H, 6.16; N, 3.11. Found: C, 66.08; H, 5.75; N, 3.25.

Photophysical measurements.

The spectrophotometric grade solvents used for photophysical experiments were purchased from VWR International and used as is. A Shimadzu UV-2501 spectrophotometer was used to record the UV−vis absorption spectra in different solvents. An HORIBA FluoroMax 4 fluorometer/phosphorometer was utilized to measure the steady-state emission spectra in different solvents. The emission quantum yields were determined by the relative actinometry method[45] in degassed solutions, in which a degassed CH_3CN solution of $[Ru(bpy)_3]Cl_2$ (Φ_{em} = 0.097, λ_{ex} = 436 nm)[46] was used as the reference for **Ir-1 – Ir-3**, and a 1 N sulfuric acid solution of quinine bisulfate (Φ_{em} = 0.546, λ_{ex} = 347.5 nm)[47] was used as the reference for ligands **6**.

The nanosecond transient difference absorption (TA) spectra and decays were measured in degassed CH_2Cl_2 solutions on an Edinburgh LP920 laser flash photolysis spectrometer. The third harmonic output (355 nm) of a Nd:YAG laser (Quantel Brilliant, pulse width = 4.1 ns, repetition rate = 1 Hz) was used as the excitation source. Each sample was purged with argon for 45 min prior to measurement. The triplet excited-state absorption coefficient (ε_T) at the TA band maximum was determined by the singlet depletion method,[48] in which the following equation was used to calculate the ε_T.[48]

$$\varepsilon_T = \frac{\varepsilon_S[\Delta OD_T]}{\Delta OD_S} \quad (1)$$

where ε_S is the ground-state molar extinction coefficient at the wavelength of the bleaching band minimum of the TA spectrum; ΔOD_S and ΔOD_T are the optical density changes at the minimum of the bleaching band and the maximum of the positive absorption band, respectively. After obtaining the ε_T value, the triplet quantum yield (Φ_T) could be determined by the relative actinometry.[49] The ΔOD of an optically matched sample solution at the excitation wavelength of 355 nm in a 1-cm cuvette was compared to that of the reference solution (SiNc in benzene) at 590 nm (ε_{590} = 70,000 L.mol^{-1}.cm^{-1}, Φ_T = 0.20)[50] using equation (2) to calculate the Φ_T.

$$\Phi_T^s = \Phi_T^{SiNc} \times \frac{\Delta OD_T^s}{\Delta OD_T^{SiNc}} \times \frac{\varepsilon_T^{SiNc}}{\varepsilon_T^s} \quad (2)$$

where the superscript s represents the samples, ΔOD is the optical density change at 590 nm, and ε_T is the triplet excited-state extinction coefficient.

The femtosecond laser pump–probe system consists of an amplified erbium-doped fiber laser, which is frequency doubled to 780 nm and amplified in a regenerative amplifier (Clark MXR CPA 2001). This femtosecond laser produces pulses with 120 fs FWHM duration and 800 mJ output energy per pulse at a repetition rate of 1 kHz. A small portion of the fundamental output pulse train is used to generate white light in a 2 mm sapphire crystal while the remaining laser light is used to frequency-double the 780 nm light in order to achieve 390 nm. For the femtosecond laser spectroscopy measurements, the excitation beam was modulated by a chopper with a 100 Hz frequency. The probe light was used with reflective optics in order to avoid white light dispersion. Measurements were

conducted with the excitation beam focused to a spot diameter of about 1 mm and the probe beam to 200 μm. For measurements in this study, the sample solutions were placed in a 2-mm path length quartz cuvette. Absorption spectra of **Ir-1** – **Ir-3** and ligand **6** were taken before and after the time-resolved experiment and no significant change was observed. All fs TA measurements were performed at room temperature.[51-57]

Nonlinear transmission experiment.

The reverse saturable absorption of **Ir-1 – Ir-3** was characterized by a nonlinear transmission experiment at 532 nm using a Quantel Brilliant laser as the light source. The pulse width of the laser was 4.1 ns, and the repetition rate was set to 10 Hz. The complexes were dissolved in CH_2Cl_2 and the concentration of the sample solutions was adjusted to obtain a linear transmission of 90% at 532 nm in a 2-mm-thick cuvette. The experimental setup and details are similar to those reported previously.[35] A 40-cm plano-convex lens was used to focus the beam to the center of the 2-mm-thick sample cuvette. The radius of the beam waist at the focal point was approximately 96 μm.

Computational methods

The ground-state geometries of **Ir-1 – Ir-3** and ligand **6** were optimized at the level of DFT, while the excited-state properties, including absorption and emission, were calculated using linear response TDDFT, as implemented in Gaussian 09 quantum chemistry software package.[58] The hybrid PBE1[59] functional was chosen to optimize the ground state geometry, which incorporates PBE nonlocal exchange and 25% of the local Hartree Fock (HF) exchange. For all calculations, the LANL2DZ basis set[60] was applied for heavy Ir ion, while the remaining atoms were modeled by 6-31G* basis set.[61] Both geometry optimization and optical property calculations were performed in dichloromethane (CH_2Cl_2, $\varepsilon_r = 9.08$) using the conductor polarized continuum model (CPCM)[62,63] implemented in Gaussian 09. Including solvent also helps to remove the spurious charge transfer states, a well-known problem of TDDFT.[64,65]

Our previous work demonstrates that the chosen methodology allows for accurate enough representations of the ground- and excited-state properties of various Ir(III) complexes.[35] We have found that optimized geometries of **Ir-1 – Ir-3** negligibly depend on the functional used in calculations. However, the excited states properties are highly sensitive to the percentage of the HF local exchange in the functional,[66] leading to either a blue-shift of the excited energy for the high-portion of HF in the functional or a red-shift for lower percentage of the HF, as compared to the experimental spectra. Therefore, we changed the HF portion in PBE1 functional to 31%, which provided the best agreement with the experimental spectra of all complexes we studied. To keep consistency, the same 31% percentage of HF was also used in the subsequent calculations of the emission energies. Interestingly, despite a constant shift of excited energies, the choice of a functional and a portion of the HF exchange in it insignificantly affect the nature of orbitals contributing to optical transitions.

For absorption spectral calculations, 40 lowest singlet excited states were calculated to reproduce the experimental spectra in the 250-600 nm range. The discrete optical transitions with their corresponding oscillator strength were broadened by a Gaussian function with the line width of 0.08 eV to represent an experimental inhomogeneous spectral broadening. To obtain the triplet (phosphorescence) and singlet (fluorescence) emission energies, the molecular structures of the lowest singlet excited (S_1) and lowest triplet excited (T_1) states were optimized using analytical TDDFT gradients,[67,68] as implemented in the Gaussian 09 software. A compact representation of an excited state via photoexcited electron-hole pair, which fits for chemical intuition, can be obtained using natural transition orbitals (NTOs).[69,70] By performing NTO calculations implemented in Gaussian 09, a single particle transition from a ground state to an excited state could be generated through unitary transformation of transition density matrix of a specific excited state, which provides an excited hole (occupied NTO) and an electron (unoccupied NTO).[69] For visualizing NTOs pairs contributing to the most important optical transitions, Chemcraft-1.7 software[71] was used for plotting excited charge densities by setting isovalue as 0.02.

Results and discussion

Molecular geometries

The optimized ground-state geometries of **Ir-1 – Ir-3** in CH_2Cl_2 at the DFT level of theory are presented in ESI Figure S1. The dihedral angles between the different parts in the C^N and N^N ligands for **Ir-1 – Ir-3** are listed in ESI Table S1. Although in principle three configurations are possible for the $Ir(ppy)_2(bpy)^+$ type molecules (see Chart 2),[72] it is well known that configuration A with the two cyclometalating carbons *cis* to each other and coplanar with the two nitrogen atoms on the diimine ligand is the commonly formed one.[20,73,74,75] Therefore, although we don't have the crystal structures to confirm the configurations of **Ir-1** – **Ir-3**, the ^{1}H-NMR spectra provided in ESI Figure S2 manifest the existence of only one isomer in our product. We believe it is reasonable to assume that **Ir-1** – **Ir-3** adopt the configuration of A. The same configuration was used for our DFT calculations.

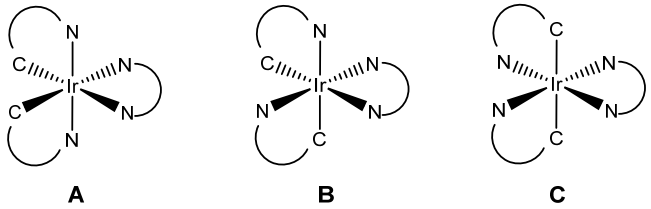

Chart 2 Possible configurations for $Ir(ppy)_2(bpy)^+$ type molecules

For optimization of the ground-state geometry of **Ir-1** – **Ir-3**, we started from planar structures for all complexes. However, upon optimization, the fluorenyl substituents at the 2-phenylpyridine (C^N) ligands are twisted from the 2-phenylpyridine plane by ~35-38^o, which are similar to those reported for the other Ir(III) complexes bearing the BTF substituted C^N ligands.[35,37,76] The NI substituents attached at the 7-position of the fluorenyl motif are also

twisted from the fluorene plane by an angle of ~ 50-53°, which are dramatically different from the dihedral angles between the benzothiazolyl substituent and the fluorenyl motif (~0-2°) in the other Ir(III) complexes bearing the BTF substituted C^N ligands.[35,37,76] In **Ir-3**, the fluorenyl substituents attached at the 5,5'-position of the bpy ligand deviate from the bpy plane by an angle of ~ 34°, and the benzothiazolyl substituents exhibit a dihedral angle of < 1° with respect to the fluorene plane, due to geometry optimization.

UV-vis absorption

The UV-vis absorption spectra of **Ir-1 – Ir-3** and the ligand **6** in a CH_2Cl_2 solution (1×10^{-5} mol/L) are depicted in Figure 1(a) and are compared to the calculated absorption spectra in Figure 1(b). More detailed information on the absorption band maxima and extinction coefficients are listed in Table 1. The calculated spectra well reproduce the two dominant absorption bands revealed in the experimental data. Both of these bands well correlate with the main absorption bands of ligand **6** (dark cyan line in Figure 1(a)). Excited-state orbitals, *i.e.* the natural transition orbitals (NTOs), corresponding to the most intensive optical transitions demonstrate that the lowest-energy transition of **6** has a hole being mostly localized on the phenylfluorene component and an electron predominantly located on the NI group (see Table 2). Therefore, the lowest-energy band (ca. 380 nm) of **6** has the predominant intraligand charge transfer (^{1}ILCT) character. Optical transitions contributing to the high-energy absorption band (ca. 296 nm) hold mostly the delocalized $^1\pi,\pi^*$ character with some admixture of ^{1}ILCT features (see NTOs for the 4th and 5th excited states in Table 2). As such, it is reasonable to assume that both optically intensive bands in **Ir-1 – Ir-3** are also dominated by the ^{1}ILCT or $^1\pi,\pi^*$ characters. Compared to ligand **6**, however, the absorption bands of Ir(III) complexes exhibit a bathochromic shift, which is more salient in complex **3**. Such a red-shift is caused by the delocalization of the ligand-center π orbitals facilitated by the Ir(III) *d* orbitals.[77]

In addition, the interactions between the ligands and the Ir(III) ion result in the appearance of the lowest energy optical transitions that contribute to the shoulder in the range of ca. 450-570 nm (see insert of Figure 1(a)). Optical transitions contributing to this shoulder predominantly arises from the hole that is hybridized over Ir(III) *d*-orbital and π-orbital of the C^N ligands to the π^* electron mostly localized on the N^N ligand, as depicted by NTOs presented in Table 3. Thus, the lowest transitions of **Ir-1 – Ir-3** are attributed to ligand-to-ligand charge transfer (^{1}LLCT) / metal-to-ligand charge transfer (^{1}MLCT) in nature. Because the most extended π-conjugation of the BTF-bpy ligand in **Ir-3** stabilizes the bpy localized π^* orbital compared to those in **Ir-1** and **Ir-2**, the lowest energy ^{1}MLCT/^{1}LLCT transitions are more red-shifted in **Ir-3**.

As demonstrated in Figure 1(a), the intensive low-energy absorption bands at ca. 380-400 nm for **Ir-1 – Ir-3** feature the similar shape and energy to that of ligand **6**. Thus, it is reasonable to assume that these bands have the similar nature as that for ligand **6**, namely predominantly ^{1}ILCT transitions from the phenylfluorene to NI component in the C^N ligand with admixture of minor $^1\pi,\pi^*$ (π(NI) → π^*(NI)) character, as discussed earlier for ligand **6**. This notion is supported by the NTOs illustrated in Table 4. However, NTOs in Table 4 reveal that contribution of ^{1}ML'CT (*d*(Ir) → π^*(NI)) transition is also noticeable in these absorption bands. Contribution of both types of transitions (^{1}ILCT/$^1\pi,\pi^*$ and ^{1}ML'CT) at the same energy interval increases the intensity and broadens the main low-energy absorption band, as compared to that in ligand **6**. In **Ir-3**, the intensive transitions at ca. 404 nm hold a predominant $^1\pi,\pi^*$/^{1}ILCT (π(BTF) → π^*(bpy)) character localized on the N^N ligand in addition to the ^{1}ILCT/$^1\pi,\pi^*$/^{1}ML'CT transitions based on the C^N ligand. The predominant contribution of the N^N ligand localized $^1\pi,\pi^*$/^{1}ILCT transitions to the low-energy absorption band in **Ir-3** causes a significant red-shift and enhanced intensity of this band in comparison to the respective bands in **Ir-1** and **Ir-2**. Similar effect has been observed in Pt(II) complexes bearing BTF functionalized bpy ligand.[41]

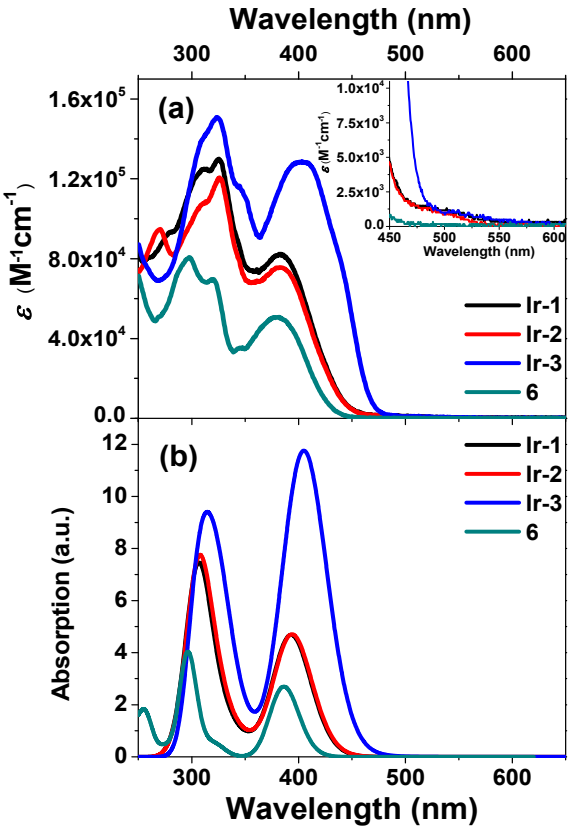

Fig. 1 The experimental (a) and calculated (b) UV-vis absorption spectra of complexes **Ir-1 – Ir-3** and ligand **6** in CH_2Cl_2. The inset in (a) is the expanded experimental spectra between 450 and 600 nm.

The other major absorption band at ca. 325 nm (experiment) in **Ir-1 – Ir-3** (which corresponds to the calculated ~ 304 – 310 nm transitions) is dominated by the $^1\pi,\pi^*$ transitions associated with the C^N ligand, as illustrated by the NTOs in Table 5. These $^1\pi,\pi^*$ transitions also have some admixture of ^{1}LLCT/^{1}MLCT characters, since an electron is partially delocalized over the N^N ligands, while the hole is hybridized with *d*-orbital of the Ir(III). Additionally, very minor signature of ^{1}ILCT transition from the phenylfluorene component to the NI component or the pyridine ring of the C^N

ligand is evident. In addition to this major absorption band, **Ir-3** has a salient shoulder at ca. 350 nm (corresponding to the calculated ~ 325 nm transitions), which contains the prevailing $^1\pi,\pi^*$ character originating from the NI component and the ^{1}ILCT character from the phenylfluorene component to the NI component. A minor ^{1}LLCT/^{1}MLCT contribution is also evident for these transitions. The predominant $^1\pi,\pi^*/^1$ILCT nature of excited orbitals contributing to this shoulder in **Ir-3** explains the higher intensity of the high-energy absorption band of **Ir-3** compared to the other two complexes.

Table 1 Photophysical data of **Ir-1 – Ir-3** and ligand **6**.

	λ_{abs}/nm (ε/10^4 L mol^{-1} cm^{-1})[a]	λ_{em}/nm (τ_0/μs; k_{sq}/L·mol^{-1}·s^{-1}; Φ_{em})[b]	$^{theor}\lambda_{phos}$ [c]/ nm	$\lambda_{T1\text{-}Tn}$/nm (τ_T/μs; $\varepsilon_{T1\text{-}Tn}$/$10^4$ L mol^{-1} cm^{-1}); Φ_T)[d]
Ir-1	311 (12.49), 324 (13.04), 383 (8.24)	606 (9.5; 4.75×10^8; 0.081)	592	485 (9.9; 16.33), 750 (9.0, 14.13); 0.037
Ir-2	311 (10.74), 325 (12.70), 381 (7.58)	600 (41.1; 5.10×10^8; 0.15)	592	485 (41.5; 19.09), 740 (40.9; 18.88); 0.034
Ir-3	306 (13.75), 323 (15.11), 404 (12.87)	609 (2.2; -; 0.18)	594	550 (2.6; 6.79), 740 (2.4; 5.86); 0.092
6	296 (8.08), 319 (6.99), 380 (5.07)	498 (-; -; 0.60)	-	450 (39.5; 5.91), 700 (38.5; 6.92); 0.10

[a]Absorption band maxima and molar extinction coefficients in CH_2Cl_2 at room temperature. [b]Room temperature emission band maxima, intrinsic lifetimes, self-quenching rate constants and emission quantum yields measured in CH_2Cl_2. A degassed CH_3CN solution of $[Ru(bpy)_3]Cl_2$ (Φ_{em} = 0.097, λ_{ex} = 436 nm) was used as the reference. [c]Calculated by TDDFT for optimized triplet geometry. [d]Nanosecond transient absorption band maxima, triplet extinction coefficients, triplet excited-state lifetimes and quantum yields measured in CH_2Cl_2 at room temperature. SiNc in C_6H_6 was used as the reference. ($\varepsilon_{590\ nm}$ = 70,000 L mol^{-1} cm^{-1}, Φ_T = 0.20).

Table 2 Natural transition orbitals (NTOs) representing the main absorption bands of ligand **6**

Excited states and properties	Hole	Electron
S_1 385 nm f = 0.765	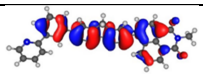	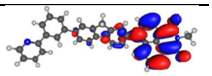
S_2 320 nm f = 0.141	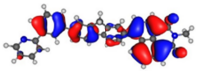	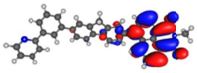
S_4 297 nm f = 0.129	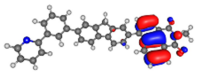 79%	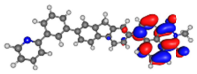 79%
	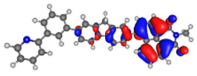 16%	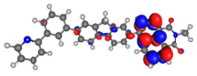 16%
S_5 296 nm f = 0.992	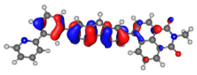	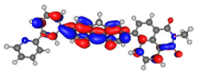

The UV-vis absorption of **Ir-1 – Ir-3** and ligand **6** in toluene, acetonitrile and acetone are also studied to evaluate the solvent dependency of the optical transitions of **Ir-1 – Ir-3** and to confirm our aforementioned assignments for the absorption bands. These results are provided in ESI Figures S4-S7. The results manifest that the polarity of solvent negligibly affects the transition energies of these complexes and ligand. This phenomenon can be accounted for by the mixed nature of various charge transfer transitions and $^1\pi,\pi^*$ transitions in the two major absorption bands.

Table 3 Natural transition orbitals (NTOs) representing the lowest energy transitions contributing to the shoulder of the 380 - 400 nm band of **Ir-1 – Ir-3**

	Excited states and properties	Hole	Electron
Ir-1	S_1 447 nm f = 0.0005	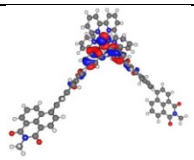	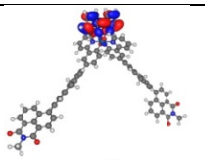
Ir-2	S_1 442 nm f = 0.0011	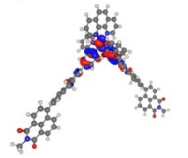	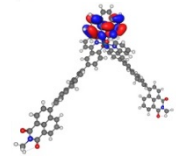
Ir-3	S_1 473 nm f = 0.0068	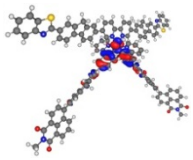	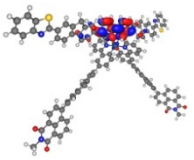

Table 4 Natural transition orbitals (NTOs) representing the main low-energy absorption bands (380 – 400 nm) of **Ir-1 – Ir-3.**

	Excited state and properties	Hole	Electron
Ir-1	S_2 394 nm $f = 0.895$	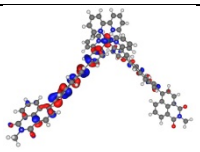 65%	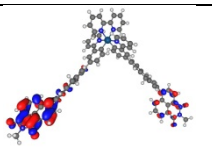 65%
		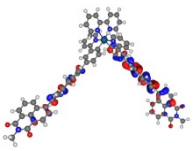 33%	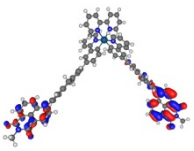 33%
	S_3 392 nm $f = 0.719$	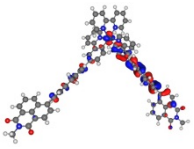 65%	 65%
		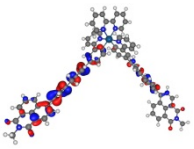 34%	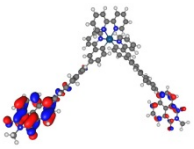 34%
Ir-2	S_3 395 nm $f = 0.830$	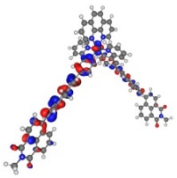 66%	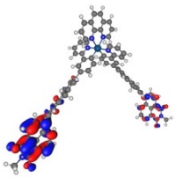 66%
		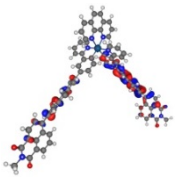 33%	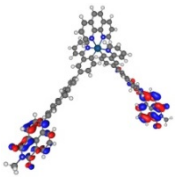 33%
	S_4 393 nm $f = 0.793$	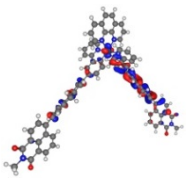 66%	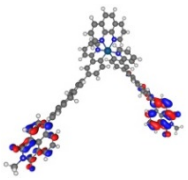 66%
		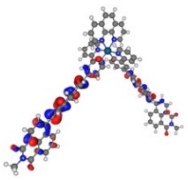 34%	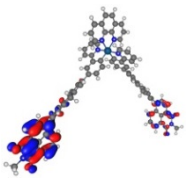 34%

Ir-3	S_2 410 nm $f = 2.862$	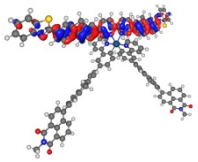	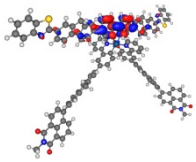
	S_4 397 nm $f = 0.869$	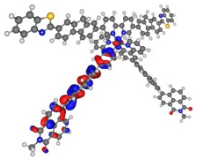	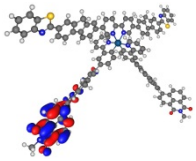
	S_5 394 nm $f = 0.806$	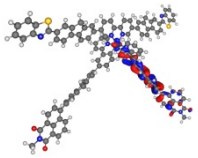	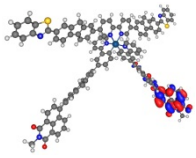

Table 5 Natural transition orbitals (NTOs) representing the high-energy major absorption bands of **Ir-1 – Ir-3**.

	Excited states and properties	Hole	Electron
Ir-1	S_{17} 310 nm $f = 1.129$	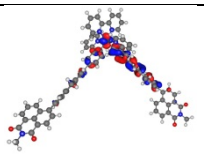 70%	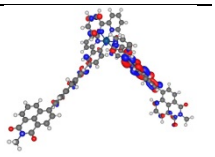 70%
		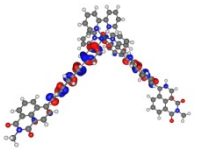 21%	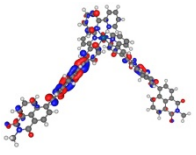 21%
	S_{20} 304 nm $f = 0.749$	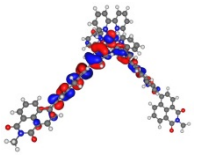 59%	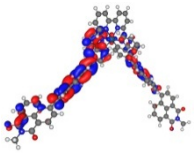 59%
Ir-2	S_{20} 307 nm $f = 0.772$	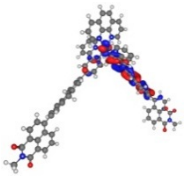 54%	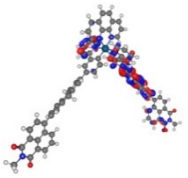 54%
		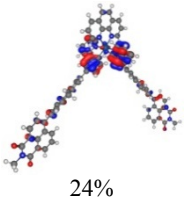 24%	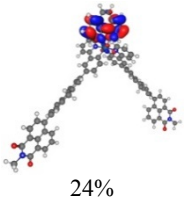 24%

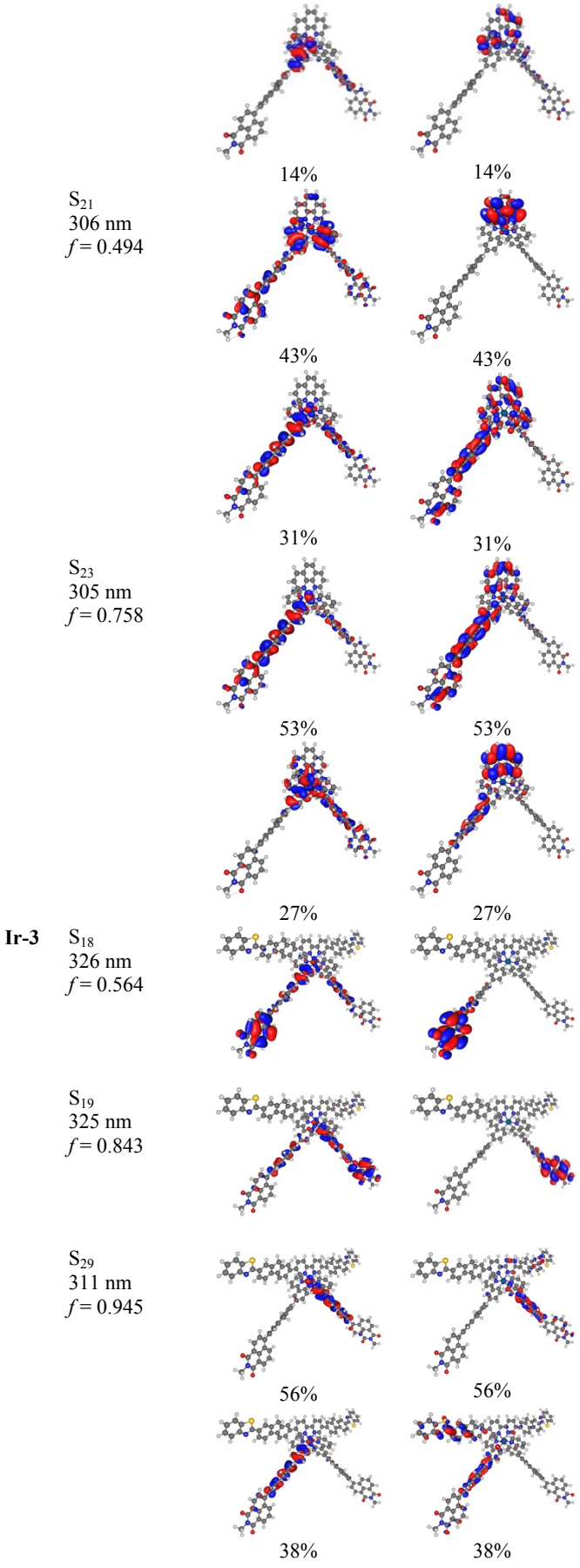

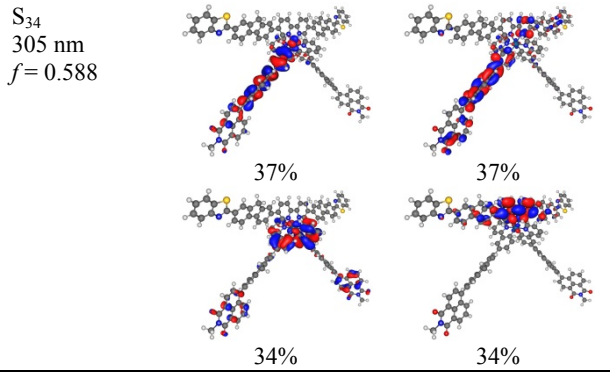

Photoluminescence

The normalized room-temperature emission spectra of **Ir-1** – **Ir-3** and ligand **6** in CH_2Cl_2 are shown in Figure 2, and the emission data are summarized in Table 1. Ligand **6** exhibits intense fluorescence in CH_2Cl_2 with the band maximum at 498 nm; while **Ir-1** – **Ir-3** exhibit much red-shifted emission at room temperature with the band maximum at 606 nm, 600 nm and 609 nm, respectively. The emission of **Ir-1** – **Ir-3** shows a significant red-shift with respect to their excitation wavelengths, and the emission lifetimes in argon saturated CH_2Cl_2 solutions are in the range of 2.2 - 41.1 μs (see Table 1). The dramatic red-shift and long lifetime of the emission of **Ir-1** – **Ir-3** suggest phosphorescence nature of the emission from these complexes. However, despite the different diimine ligands in these complexes, the emission energies of **Ir-1** – **Ir-3** are quite similar. This implies that the emission of **Ir-1** – **Ir-3** probably originates from the same structural component, likely the substituted C^N ligands.

This assumption is confirmed by the calculated NTOs contributing to the lowest-energy triplet transition, as depicted in Table 6. All complexes have the lowest energy triplet state of the exclusive $^3\pi,\pi^*$ character associated with the fluorenylnaphthalimide component at one of the C^N ligands. In contrast, the lowest-energy singlet state of **Ir-1** and **Ir-3** has the ^{1}LLCT/^{1}MLCT character with the electron being mostly located at the N^N ligand, and the hole being delocalized on the phenylfluorene motif of the C^N ligand and on the *d*-orbital of the Ir(III) ion. For **Ir-2**, the lowest-energy singlet state has the predominant fluorenylnaphthalimide localized $^1\pi,\pi^*$ character with some admixture of ^{1}MLCT/^{1}ILCT characters. The splitting between the singlet and triplet states is the largest for **Ir-2** and is the smallest for **Ir-3**. This feature along with the different origins of the lowest singlet excited state for **Ir-2** and **Ir-3** may explain the dramatically different emission lifetimes of **Ir-2** and **Ir-3** due to a weaker mixture between the singlet and triplet states in **Ir-2** but a stronger mixture in **Ir-3** when spin-orbit coupling is taking into account.

To further understand the nature of the emission in **Ir-1** – **Ir-3** and ligand **6**, the emission of these compounds is studied in different solvents. As shown in ESI Figure S8 and Table S3, ligand **6** shows a positive solvatochromic effect when the polarity of the solvent increases. This is consistent with the ^{1}ILCT/$^1\pi,\pi^*$ nature (see the calculated NTOs contributing to the lowest-energy singlet transition depicted in ESI Table S4, which shows a major contribution from

the ^{1}ILCT transition) of the fluorescence for ligand **6**. In contrast, the emission spectra of **Ir-1 – Ir-3** demonstrate a minor solvatochromic effect in different solvents as shown in ESI Figures S9-S11 and Table S3. This is consistent with the $^3\pi,\pi^*$ nature for the emission of these complexes.

The emission of complexes at room temperature is concentration dependent. Although the emission intensity keeps increasing in the concentration range of 2×10^{-6} to 1×10^{-4} mol/L for **Ir-1** and **Ir-2**, as shown in ESI Figures S12 and S13, the emission lifetime keeps decreasing with increased concentration. This indicates the occurrence of self-quenching in the concentration range studied for these two complexes. The self-quenching rate constants are deduced from the slopes of the Stern-Volmer plots and listed in Table 1. For **Ir-3**, the emission intensity increases in the concentration range of 2×10^{-6} to 1×10^{-5} mol/L, but decreases when the concentration is higher than 1×10^{-5} mol/L (see ESI Figure S14). However, the lifetime remains the same at different concentrations, implying the absence of self-quenching in **Ir-3**. This can be explained by the additional branched alkyl groups on the substituted N^N ligand, which help reduce the intermolecular interactions and prevent self-quenching. Considering the distinctively higher ground-state absorption at the excitation wavelength (λ_{ex} = 450 nm) for **Ir-3**, the observed decrease of the emission intensity at high concentrations should emanate from the inner-filter effect,[78] which could also present in **Ir-1** and **Ir-2**, but with a much smaller effect because of the much smaller molar extinction coefficients at 450 nm for **Ir-1** and **Ir-2** compared to that of **Ir-3**.

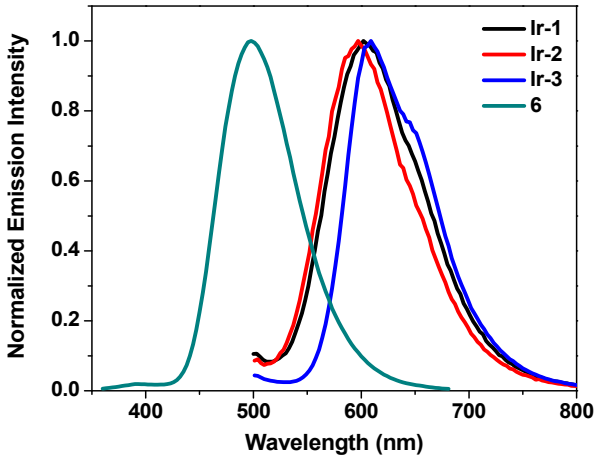

Fig. 2 Normalized emission spectra of **Ir-1 – Ir-3** (λ_{ex} = 450 nm) and ligand **6** (λ_{ex} = 379 nm) in CH_2Cl_2 solutions ($c = 1 \times 10^{-5}$ mol/L) at room temperature.

Table 6 NTOs contributing to the photoluminescence transitions corresponding to the lowest triplet excited-state energies and lowest singlet excited-state energies for **Ir-1 – Ir-3**.

	T_1 (nm)	Electron	Hole	S_1 (nm)	Electron	Hole
Ir-1	592			557		
Ir-2	592			482		
Ir-3	594			575		

Transient absorption (TA)

Many heteroleptic Ir(III) complexes have been reported to possess broad and moderately strong triplet excited-state absorption in the visible to near-IR region,[25,26,35-37] which is an important feature for an ideal reverse saturable absorber. To evaluate the feasibility of **Ir-1 – Ir-3** as potential reverse saturable absorbers, the excited-state absorption spectra, the excited-state lifetimes and the triplet excited-state quantum yields should be assessed. Therefore, the ns and fs transient absorption (TA) spectra of these complexes and ligand have been investigated.

The nanosecond TA spectra of **Ir-1 – Ir-3** and ligand **6** at zero delay after excitation in degassed CH_2Cl_2 solutions are illustrated in Figure 3, and the time-resolved spectra are provided in the Supporting Information Figures S16-19. The TA spectrum of ligand **6** features two major absorption bands, a stronger one between 400 and 600 nm and a weaker but much broader one above 600 nm. In addition, bleaching occurs between 360 and 400 nm, which coincides with the ^{1}ILCT band in its UV-vis absorption spectrum. Compared to the TA spectrum of the ligand, the spectra of **Ir-1 – Ir-3** exhibit similar features but with an obvious red-shift, indicating electron delocalization induced by the interaction of the Ir(III) center with the ligand. For all complexes, bleaching occurs at $\lambda < 425$ nm, which is consistent with the position of the low-energy major absorption band in their respective UV−vis absorption spectrum. The triplet lifetimes deduced from the decay of the TA (Table 1) for these complexes are similar to those obtained from the decay of emission, suggesting that the observed TA could arise from the same excited state that emits or an excited state that is in equilibrium with the emitting state. Considering the similar features of the TA of these complexes to that of the ligand and the similar lifetimes to those of emission, we tentatively assign the observed TA to the C^N ligand localized $^3\pi,\pi^*$ state.

One point worthy of mention is that the TA spectrum of **Ir-2** is much broader (see the comparison in ESI Figure S20) and long-lived (τ_T = 41.5 μs in CH_2Cl_2) in comparison to that of its corresponding Ir(III) complex with benzothiazolyl substituent on the C^N ligand (*i.e.* complex **4** in reference 37 with τ_{em} = 12.9 μs in CH_2Cl_2 and τ_T = 11.3 μs in toluene).[37] The similar phenomenon has been reported for the Pt(II) complexes with naphthalimidyl substituted fluorenylacetylide ligands.[40]

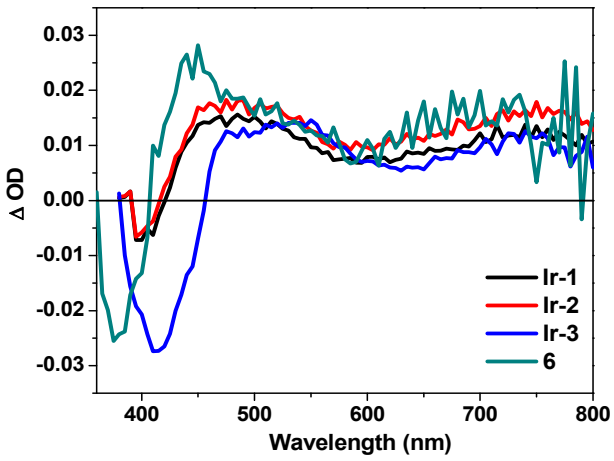

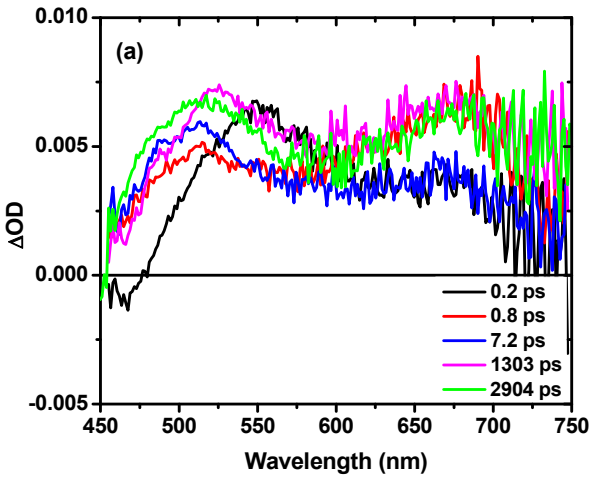

Fig. 3 Nanosecond transient differential absorption spectra of **Ir-1 – Ir-3** and ligand **6** in degassed CH_2Cl_2 solution at zero time delay after excitation. λ_{ex} = 355 nm, $A_{355\ nm}$ = 0.4 in a 1-cm cuvette.

To further understand the singlet excited-state characteristics, femtosecond TA spectra and kinetics of **Ir-1 – Ir-3** and ligand **6** were investigated. The time-resolved TA spectra of **Ir-1** and the decay profile at 675 nm are illustrated in Figure 4. Right after the 390 nm excitation (*i.e.* at 0.2 ps delay), the complex exhibits a broad transient absorption with band maxima at 550 nm and 675 nm, respectively. Then, the 550 nm band rapidly decays within 1 ps and blue-shifts to 515 nm, accompanied by the increase and a slight red-shift of the 675 nm band. At approximately 1.3 ns after excitation, the TA signals reach the maximum. After that, the TA decays slowly, and the shape of the TA spectrum resembles that of the ns TA spectrum. Fitting of the kinetics at 675 nm reveals that this complex possesses a rapid decay of 1.55±0.28 ps, a rise time of 142±22 ps, and a long-lived component that could not be fitted within the first 3 ns. Considering the nature of the 390 nm band as discussed in the previous section, we tentatively attribute the initial rapid decay to the decay of the ^{1}ILCT state to the lowest singlet excited state (^{1}LLCT/^{1}MLCT); while the 142 ps lifetime could be ascribed to the decay of the ^{1}LLCT/^{1}MLCT state including intersystem crossing to the $^3\pi,\pi^*$ state. The longer lifetime that exceeds the limit of the fs TA spectrometer should be due to the decay of the triplet excited state. **Ir-2** exhibits the similar spectral features and kinetics as those of **Ir-1** (see ESI Figure S21), with a rapid decay of 1.03±0.14 ps, a rise time of 135±18 ps, and a long-lived component of > 3 ns.

In contrast to **Ir-1** and **Ir-2**, the fs TA spectrum of **Ir-3** (Figure S22 of ESI) does not show any observable changes within the first 3 ns, with a rise time of 1.43±0.25 ps and a long-lived component when monitored at 536 nm. The TA spectral feature is similar to that of the ns TA spectrum. This implies that the intersystem crossing of **Ir-3** is ultrafast, probably due to the smaller separation between the lowest singlet and triplet excited states in this complex compared to those in **Ir-1** and **Ir-2**.

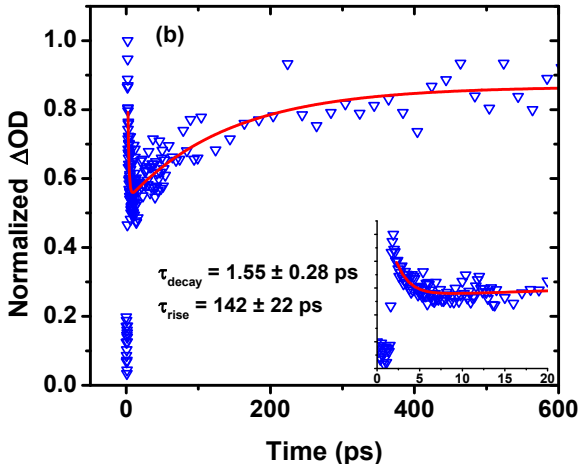

Fig. 4 (a) Femtosecond time-resolved TA spectra of **Ir-1** in CH_2Cl_2. The sample was excited with 390 nm and a power of 0.61 mW. (b) Normalized fs TA kinetics of **Ir-1** at 675 nm. The inset shows the fit of the initial decay within the first 20 ps after excitation.

Reverse saturable absorption (RSA)

The fs and ns TA show that **Ir-1 – Ir-3** all possess stronger excited-state absorption than that of the ground state at 532 nm, as manifested by the positive absorption at this wavelength. Meanwhile, the triplet excited-state lifetimes for these complexes are much longer than the nanosecond laser pulse width (4.1 ns). These features provide the necessary conditions for RSA to occur for a nanosecond laser pulse at 532 nm. To verify this, nonlinear transmission experiments were conducted for **Ir-1 – Ir-3** in CH_2Cl_2 solutions at a linear transmittance of 90% in a 2-mm cuvette using 4.1 ns, 532 nm laser pulses. The results are shown in Figure 5. When the incident energy increases, all of the complexes exhibit remarkable transmission decrease, indicative of the occurrence of strong RSA. The strength of the transmission decrease follows this trend: **Ir-2** > **Ir-3** > **Ir-1**.

To rationalize the observed transmission decrease trend for **Ir-1 – Ir-3**, the key parameters that determine the strength of RSA for ns pulses at 532 nm, *i.e.* the triplet quantum yield and the ratio of the excited-state absorption cross section to that of the ground state (σ_{ex}/σ_o), have to be evaluated. The detailed procedure for estimation of the σ_{ex}/σ_o values of **Ir-1 – Ir-3** follows that described by our group previously.[35,41] The σ_0 values at 532 nm can be calculated from the ground-state absorption molar extinction coefficients (ε) using equation $\sigma = 3.82 \times 10^{-21}\varepsilon$. The σ_{ex} value at 532 nm can be estimated from the ΔOD of the ns TA at zero time delay at 532 nm and at the TA band maximum (λ_{T1-Tn}), the ground-state absorbance (A) at 532 nm and at the TA band maximum of the same solution used for the TA measurement, and the ε_{T1-Tn} at the TA band maximum, as well as the conversion equation $\sigma = 3.82 \times 10^{-21}\varepsilon$. The obtained σ_{ex} and σ_0 values as well as the ratios of σ_{ex}/σ_0 are listed in Table 7. For RSA of ns laser pulses, the triplet quantum yield Φ_T also plays an important role in the triplet excited-state absorption. Therefore, the combined ratios of $\Phi_T\sigma_{ex}/\sigma_0$ for **Ir-1 – Ir-3** should be taken into account. As listed in Table 7, the $\Phi_T\sigma_{ex}/\sigma_0$ values correlate with the observed trend of the transmission signal decrease for **Ir-1 – Ir-3** very well. A more quantitative analysis of the RSA results and comparison to the other reported reverse saturable absorbers require a Z-scan study, which will be carried out in the future. Nonetheless, this preliminary study demonstrates that **Ir-1 – Ir-3** exhibit strong RSA at 532 nm. Considering their broadband excited-state absorption in the visible to the near-IR region and the long-lived triplet excited states, these complexes could potentially be used as broadband reverse saturable absorbers, both spectrally and temporally. This result also indicates that extending the π-conjugation of the N^N ligand could enhance the RSA of the Ir(III) complexes, as manifested by the slightly stronger RSA of **Ir-2** and **Ir-3** in comparison to that of **Ir-1**.

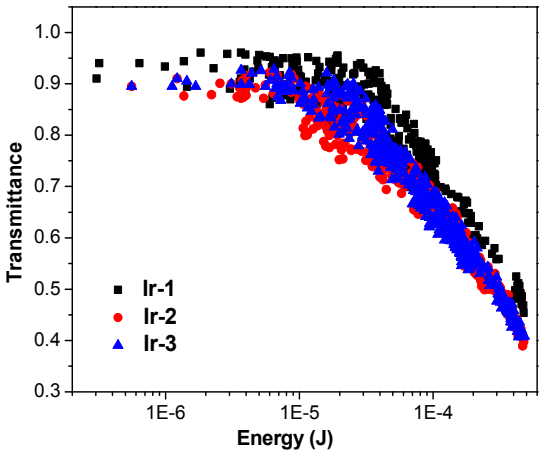

Fig. 5 Transmittance *vs.* incident energy curves for **Ir-1 – Ir-3** in CH_2Cl_2 for 4.1 ns laser pulses at 532 nm in a 2-mm cuvette. The linear transmission was adjusted to 90% for each sample in the 2-mm cuvette. The radius of the beam waist at the focal point was ~ 96 μm.

Table 7 Ground-state (σ_0) and excited-state (σ_{ex}) absorption cross sections of **Ir-1 – Ir-3** in CH_2Cl_2 at 532 nm.

Complex	**1**	**2**	**3**
$\sigma_0/10^{-18}$ cm^2	1.91	0.64	2.55
$\sigma_{ex}/10^{-18}$ cm^2	496	596	289
σ_{ex}/σ_0	260	931	113
$\Phi_T\sigma_{ex}/\sigma_0$	9.6	32	10

Conclusions

Three new Ir(III) complexes with cyclometalating 2-[3-(7-naphthalimidylfluoren-2′-yl)phenyl]pyridine ligands were synthesized and their photophysical properties were systematically investigated. All complexes have two strong absorption bands between 290 nm and 450 nm, with the low-energy band (350 – 450 nm) predominantly from the ^{1}ILCT (π(phenylfluorene) → π^*(NI)) / $^1\pi,\pi^*$ (π(NI) → π^*(NI)) / ^{1}ML'CT (d(Ir) → π^*(NI)) transitions but

admixing with $^1\pi,\pi^*$ (π(bpy) → π^*(bpy)) / ^{1}ILCT (π(benzothiazolylfluorene) → π^*(bpy)) configurations in **Ir-3**. Due to the involvement of the $^1\pi,\pi^*/^1$ILCT transitions, the low-energy band of **Ir-3** is much broader, red-shifted and more intense than the corresponding bands in **Ir-1** and **Ir-2**. The high-energy main absorption bands at ~320 nm for **Ir-1 – Ir-3** are dominated by the C^N ligand-localized $^1\pi,\pi^*$ transitions, mixed with some ^{1}LLCT/^{1}MLCT characters and minor ^{1}ILCT signature. In addition, **Ir-3** possesses a shoulder at ca. 350 nm that mainly arises from the $^1\pi,\pi^*/^1$ILCT transitions associated with the NI component, and mixed with some ^{1}LLCT/^{1}MLCT characters. The emission of **Ir-1 – Ir-3** in CH_2Cl_2 emanates from the C^N ligand-localized $^3\pi,\pi^*$ state based on the TDDFT calculations and the minor solvatochromic effect. These emitting excited states also give rise to broadband triplet excited-state absorption in the visible to near-IR region (*i.e.* 420–800 nm for **Ir-1** and **Ir-2**, and 460–800 nm for **Ir-3**). The fs TA studies reveal that **Ir-1** and **Ir-2** possess a rapid decay within 2 ps after 390 nm excitation, possibly due to the decay of the ^{1}ILCT state to the lowest-energy ^{1}MLCT/^{1}LLCT state, followed by a rising time within 150 ps, likely attributed to the decay of the ^{1}MLCT/^{1}LLCT state (including intersystem crossing to the $^3\pi,\pi$ state) after excitation. For **Ir-3**, the decay of the ^{1}MLCT/^{1}LLCT state completes within 2 ps. The stronger excited-state absorption of these complexes compared to the ground-state absorption in the visible spectral range leads to strong reverse saturable absorption (RSA) at 532 nm for ns laser pulses and the trend of transmission signal decrease follows **Ir-2** > **Ir-3** > **Ir-1**, which correlates well to the combined parameters of the ratio of the excited-state absorption cross section to that of the ground state (σ_{ex}/σ_0) and the triplet excited-state quantum yield (Φ_T). Our studies reveal that extending the π-conjugation of the N^N ligand can increase the strength of RSA slightly. In addition, in comparison to the respective Ir(III) complexes with benzothiazolyl substituent on the C^N ligand, the naphthalimidyl substitution on the C^N ligand dramatically increases the triplet excited-state lifetimes and broadens the triplet excited-state absorption to the NIR region, which could make **Ir-1 – Ir-3** broadband reverse saturable absorbers.

Acknowledgments

This work is partially supported by the Army Research Laboratory (W911NF-10-2-0055) for the materials synthesis and characterization and partially supported by the National Science Foundation (CNS-1229316 and DMR-1411086) for the computational work to W. Sun. S. Kilina acknowledges the U.S. Department of Energy Early-Career Grant DESC008446 for partial financial support and the Center for Computationally Assisted Science and Technology (CCAST) at North Dakota State University for computer access and administrative support.

Notes and references

[a]*Department of Chemistry and Biochemistry, North Dakota State University, Fargo, North Dakota 58108-6050, United States. E-mail: Wenfang.Sun@ndsu.edu. Phone: 701-231-6254. Fax: 701-231-8831. Svetlana.Kilina@ndsu.edu*

[b]*Materials and Nanotechnology Program, North Dakota State University, Fargo, North Dakota 58108, United States.*

[c]*Department of Chemistry, Case Western Reserve University, Cleveland, Ohio 44106, United States. E-mail:* clemens.burda@case.edu.

Electronic Supplementary Information (ESI) available: The optimized geometries of **Ir-1 – Ir-3** in CH_2Cl_2 via DFT calculations, the ^{1}H-NMR spectra of **Ir-1 – Ir-3** in $CDCl_3$, the comparison of the experimental and calculated UV-vis absorption spectra of **Ir-1 – Ir-3** and ligand **6** in CH_2Cl_2, the absorption spectra and emission spectra of **Ir-1 – Ir-3** and ligand **6** in different solvents, the concentration dependent emission spectra and the time-resolved nanosecond transient absorption spectra of **Ir-1 – Ir-3** and ligand **6** in CH_2Cl_2, the time-resolved fs TA spectra and kinetics of **Ir-2** and **Ir-3** and ligand **6** in CH_2Cl_2, the emission parameters of **Ir-1 – Ir-3** and ligand **6** in different solvents, the additional NTOs for the UV-vis absorption of ligand **6**, and NTOs contributing to the fluorescence transition from the lowest singlet excited state to the singlet ground state for ligand **6**. See DOI: 10.1039/b000000x/

References

1. L. M. Vogler and K. J. Brewer, *Inorg. Chem.*, 1996, **35**, 818-824.
2. J. A. Treadway, B. Loeb, R. Lopez, P. A. Anderson, F. R. Keene and T. J. Meyer, *Inorg. Chem.*, 1996, **35**, 2242-2246.
3. S. Lamansky, P. Djurovich, D. Murphy, F. Abdel-Razzaq, R. Kwong, I. Tsyba, M. Bortz, B. Mui, R. Bau and M. E. Thompson, *Inorg. Chem.*, 2001, **40**, 1704-1711.
4. S. Lamansky, P. Djurovich, D. Murphy, F. Abdel-Razzaq, H.-E. Lee, C. Adachi, P. E. Burrows, S. R. Forrest and M. E. Thompson, *J. Am. Chem. Soc.*, 2001, **123**, 4304-4312.
5. F. Neve, A. Crispini, S. Campagna and S. Serroni, *Inorg. Chem.*, 1999, **38**, 2250-2258.
6. A. Dovletoglou, S. A. Adeyemi and T. J. Meyer, *Inorg. Chem.*, 1996, **35**, 4120-4127.
7. M. G. Colombo, A. Hauser and H. U. Guedel, *Inorg. Chem.*, 1993, **32**, 3088-3092.
8. P. J. Hay, *J. Phys. Chem. A*, 2002, **106**, 1634-1641.
9. J. I. Goldsmith, W. R. Hudson, M. S. Lowry, T. H. Anderson and S. Bernhard, *J. Am. Chem. Soc.*, 2005, **127**, 7502-7510.
10. L. L. Tinker, N. D. McDaniel, P. N. Curtin, C. K. Smith, M. J. Ireland and S. Bernhard, *Chem. Eur. J.*, 2007, **13**, 8726-8732.
11. E. I. Mayo, K. Kilså, T. Tirrell, P. I. Djurovich, A. Tamayo, M. E. Thompson, N. S. Lewis and H. B. Gray, *Photochem. Photobiol. Sci.*, 2006, **5**, 871-873.
12. E. Baranoff, J. H. Yum, I. Jung, R. Vulcano, M. Grätzel and M. Nazeeruddin, *Chem. Asian J.*, 2010, **5**, 496-499.
13. Y. Shinpuku, F. Inui, M. Nakai and Y. Nakabayashi, *J. Photochem. Photobiol. A: Chem.*, 2011, **222**, 203-209.
14. Y. Sun, N. C. Giebink, H. Kanno, B. Ma, M. E. Thompson and S. R. Forrest, *Nature*, 2006, **440**, 908-912.
15. W.-Y. Wong and C.-L. Ho, *Coord. Chem. Rev.*, 2009, **253**, 1709-1758.
16. P. Kang, C. Cheng, Z. Chen, C. K. Schauer, T. J. Meyer and M. Brookhart, *J. Am. Chem. Soc.*, 2012, **134**, 5500-5503.
17. J. F. Hull, D. Balcells, J. D. Blakemore, C. D. Incarvito, O. Eisenstein, G. W. Brudvig and R. H. Crabtree, *J. Am. Chem. Soc.*, 2009, **131**, 8730-8731.
18. J. F. Hull, Y. Himeda, W.-H. Wang, B. Hashiguchi, R. Periana, D. J. Szalda, J. T. Muckerman and E. Fujita, *Nat. Chem.*, 2012, **4**, 383-388.
19. S. Sato, T. Morikawa, T. Kajino and O. Ishitani, *Angew. Chem. Int. Ed.*, 2013, **52**, 988-992.
20. Q. Zhao, S. Liu, M. Shi, C. Wang, M. Yu, L. Li, F. Li, T. Yi and C. Huang, *Inorg. Chem.*, 2006, **45**, 6152-6160.
21. S. Ladouceur, D. Fortin and E. Zysman-Colman, *Inorg. Chem.*, 2010, **49**, 5625-5641.

22. F. Neve, M. La Deda, A. Crispini, A. Bellusci, F. Puntoriero and S. Campagna, *Organometallics*, 2004, **23**, 5856-5863.
23. S. Ladouceur, D. Fortin and E. Zysman-Colman, *Inorg. Chem.*, 2011, **50**, 11514-11526.
24. R. D. Costa, F. Monti, G. Accorsi, A. Barbieri, H. J. Bolink, E. Ortí and N. Armaroli, *Inorg. Chem.*, 2011, **50**, 7229-7238.
25. Y. Liu, S. Jiang and K. S. Schanze, *Chem. Commun.*, 2003, 650-651.
26. K.-Y. Kim, R. T. Farley and K. S. Schanze, *J. Phys. Chem. B*, 2006, **110**, 17302-17304.
27. X. S. Zeng, M. Tavasli, I. F. Perepichka, A. S. Batsanov, M. R. Bryce, C. J. Chiang, C. Rothe, A. P. Monkman, *Chem. Eur. J.* 2008, **14**, 933-943.
28. S.-J. Liu, Z.-H. Lin, Q. Zhao, Y. Ma, H.-F. Shi, M.-D. Yi, Q.-D. Ling, Q.-L. Fan, C.-X. Zhu, E.-T. Kang, W. Huang, *Adv. Funct. Mater.* 2011, **21**, 979-985.
29. S.-J. Liu, Q. Zhao, R.-F. Chen, Y. Deng, Q.-L. Fan, F.-Y. Li, L.-H. Wang, C.-H. Huang, W. Huang, *Chem. Eur. J.* 2006, **12**, 4351-4361.
30. S.-J. Liu, Q. Zhao, Y. Deng, Y.-J. Xia, J. Lin, Q.-L. Fan, L.-H. Wang, W. Huang, *J. Phys. Chem. C*, 2007, **111**, 1166-1175.
31. Y. Deng, S.-J. Liu, Q.-L. Fan, C. Fang, R. Zhu, K.-Y. Pu, L.-H. Yuwen, L.-H. Wang, W. Huang, *Synth. Met.* 2007, **157**, 813-822.
32. W.-Y. Wong, G.-J. Zhou, X.-M. Yu, H.-S. Kwok, B.-Z. Tang, *Adv. Funct. Mater.* 2006, **16**, 838-846.
33. W.-Y. Wong, G.-J. Zhou, X.-M. Yu, H.-S. Kwok, Z. Lin, *Adv. Funct. Mater.* 2007, **17**, 315-323.
34. X.-M. Yu, H.-S. Kwok, W.-Y. Wong, G.-J. Zhou, *Chem. Mater.* 2006, **18**, 5097-5103.
35. Y. Li, N. Dandu, R. Liu, L. Hu, S. Kilina and W. Sun, *ACS Appl. Mater. Interfaces*, 2013, **5**, 6556-6570.
36. R. Liu, N. Dandu, Y. Li, S. Kilina and W. Sun, *Dalton Trans.*, 2013, **42**, 4398-4409.
37. Y. Li, N. Dandu, R. Liu, Z. Li, S. Kilina and W. Sun, *J. Phys. Chem. C*, 2014, **118**, 6372-6384.
38. H. Guo, S. Ji, W. Wu, W. Wu, J. Shao and J. Zhao, *Analyst*, 2010, **135**, 2832-2840.
39. H. Guo, M. L. Muro-Small, S. Ji, J. Zhao and F. N. Castellano, *Inorg. Chem.*, 2010, **49**, 6802-6804.
40. R. Liu, A. Azenkeng, Y. Li and W. Sun, *Dalton Trans.*, 2012, **41**, 12353-12357.
41. Y. Li, R. Liu, E. Badaeva, S. Kilina and W. Sun, *J. Phys. Chem. C*, 2013, **117**, 5908-5918.
42. E. P. Woo, M. Inbasekaran, W. Shiang and G. R. Roof, *Int. Pat. Appl. WO 97/05184*, 1997.
43. H. Liu, B. Qu, J. Chen, Z. Cong, Z. An, C. Gao, L. Xiao, Z. Chen and Q. Gong, *J. Appl. Polym. Sci.*, 2013, **128**, 3250-3255.
44. S.-O. Kim, Q. Zhao, K. Thangaraju, J. J. Kim, Y.-H. Kim and S.-K. Kwon, *Dyes Pigm.*, 2011, **90**, 139-145.
45. J. N. Demas and G. A. Crosby, *J. Phys. Chem.*, 1971, **75**, 991-1024.
46. K. Suzuki, A. Kobayashi, S. Kaneko, K. Takehira, T. Yoshihara, H. Ishida, Y. Shiina, S. Oishi and S. Tobita, *Phys. Chem. Chem. Phys.*, 2009, **11**, 9850-9860.
47. D. F. Eaton, *Pure Appl. Chem.*, 1988, **60**, 1107-1114.
48. I. Carmichael and G. L. Hug, *J. Phys. Chem. Ref. Data*, 1986, **15**, 1-250.
49. C. V. Kumar, L. Qin and P. K. Das, *J. Chem. Soc., Faraday Trans. 2: Mol. Chem. Phys.*, 1984, **80**, 783-793.
50. P. A. Firey, W. E. Ford, J. R. Sounik, M. E. Kenney and M. A. Rodgers, *J. Am. Chem. Soc.*, 1988, **110**, 7626-7630.
51. C. Burda, S. Link, T. Green and M. El-Sayed, *J. Phys. Chem. B*, 1999, **103**, 10775-10780.
52. C. Burda and M. A. El-Sayed, *Pure Appl. Chem.*, 2000, **72**, 165-177.
53. C. Burda, S. Link, M. B. Mohamed and M. El-Sayed, *J. Chem. Phys.*, 2002, **116**, 3828-3833.
54. Y. Lou, X. Chen, A. C. Samia and C. Burda, *J. Phys. Chem. B*, 2003, **107**, 12431-12437.
55. Y. Lou, A. C. Samia, J. Cowen, K. Banger, X. Chen, H. Lee and C. Burda, *Phys. Chem. Chem. Phys.*, 2003, **5**, 1091-1095.
56. C.-H. Chuang, S. S. Lo, G. D. Scholes and C. Burda, *J. Phys. Chem. Lett.*, 2010, **1**, 2530-2535.
57. C.-H. Chuang, T. L. Doane, S. S. Lo, G. D. Scholes and C. Burda, *ACS Nano*, 2011, **5**, 6016-6024.
58. M. J. Frisch, G. W. Trucks, H. B. Schlegel, G. E. Scuseria, M. A. Robb, J. R. Cheeseman, G. Scalmani, V. Barone, B. Mennucci, G. A. Petersson, H. Nakatsuji, M. Caricato, X. Li, H. P. Hratchian, A. F. Izmaylov, J. Bloino, G. Zheng, J. L. Sonnenberg, M. Hada, M. Ehara, K. Toyota, R. Fukuda, J. Hasegawa, M. Ishida, T. Nakajima, Y. Honda, O. Kitao, H. Nakai, T. Vreven, Jr. J. A. Montgomery, J. E. Peralta, F. Ogliaro, M. Bearpark, J. J. Heyd, E. Brothers, K. N. Kudin, V. N. Staroverov, R. Kobayashi, J. Normand, K. Raghavachari, A. Rendell, J. C. Burant, S. S. Iyengar, J. Tomasi, M. Cossi, N. Rega, N. J. Millam, M. Klene, J. E. Knox, J. B. Cross, V. Bakken, C. Adamo, J. Jaramillo, R. Gomperts, R. E. Stratmann, O. Yazyev, A. J. Austin, R. Cammi, C. Pomelli, J. W. Ochterski, R. L. Martin, K. Morokuma, V. G. Zakrzewski, G. A. Voth, P. Salvador, J. J. Dannenberg, S. Dapprich, A. D. Daniels, Ö. Farkas, J. B. Foresman, J. V. Ortiz, J. Cioslowski and D. J. Fox, *Gaussian 09*, Revision A.1, Gaussian, Inc. Wallingford CT, 2009.
59. J. P. Perdew, K. Burke and M. Ernzerhof, *Phys. Rev. Lett.*, 1996, **77**, 3865.
60. P. J. Hay and W. R. Wadt, *J. Chem. Phys.*, 1985, **82**, 299-310.
61. C. Adamo and V. Barone, *J. Chem. Phys.*, 1999, **110**, 6158-6170.
62. V. Barone, M. Cossi and J. Tomasi, *J. Comput. Chem.*, 1998, **19**, 404-417.
63. M. Cossi, V. Barone, R. Cammi, J. Tomasi, *Chem. Phys. Lett.* 1996**, 255**, 327-335.
64. E. Badaeva, V. V. Albert, S. Kilina, A. Koposov, M. Sykora and S. Tretiak, *Phys. Chem. Chem. Phys.*, 2010, **12**, 8902-8913.
65. V. V. Albert, E. Badaeva, S. Kilina, M. Sykora, S. Tretiak, *J. Luminescence* 2011**, 131**, 1739-1746.
66. F. Jensen, *Introduction to Computational Chemistry*, (1st edition), John Wiley & Sons Ltd, Chichester, England, 1999, pp 177-193.
67. C. Van Caillie and R. D. Amos, *Chem. Phys. Lett.*, 2000, **317**, 159-164.
68. F. Furche and R. Ahlrichs, *J. Chem. Phys.*, 2002, **117**, 7433-7447.
69. R. L. Martin, *J. Chem. Phys.*, 2003, **118**, 4775-4777.
70. E. R. Batista and R. L. Martin, "Natural transition orbitals" in *Encyclopedia of Computational Chemistry,* von Ragu Schleyer, P.; Allinger, N. L.; Clark, T.; Gasteiger, J.; Kollman, P. A.; Schaefer, H. F. III; Schreiner, P. R. eds. John Wiley & Sons Ltd., Chichester, U. K., 2004.
71. G. A. Zhurko, D. A. Zhurko, Chemcraft (Version 1.7) 2013, http://www.chemcraftprog.com.
72. L. Flamigni, A. Barbieri, C. Sabatini, B. Ventura and F. Barigelletti, *Top. Curr. Chem.*, 2007, **281**, 143-203.
73. M. Maestri, V. Balzani, C. Deuschel-Cornioley and A. von Zelewsky, *Adv. Photochem.*, 1992, **17**, 1-68.
74. F. O. Garces, K. A. King and R. J. Watts, *Inorg. Chem.*, 1988, **27**, 3464-3471.
75. L. Donato, C. E. McCusker, F. N. Castellano and E. Zysman-Colman, *Inorg. Chem.* 2013, **52**, 8495-8504.
76. R. Liu, N. Dandu, J. Chen, Y. Li, Z. Li, S. Liu, C. Wang, S. Kilina, B. Kohler and W. Sun, *J. Phys. Chem. C*, 2014, **118**, 23233-23246.
77. K. Haskins-Glusac, I. Ghiviriga, K. A. Abboud and K. S. Schanze, *J. Phys. Chem. B*, 2004, **108**, 4969-4978.
78. M. Kubista, R. Sjöback, S. Eriksson and B. Albinsson, *Analyst*, 1994, **119**, 417-419.

Table of Content Synopsis

Three cationic Ir(III) complexes with cyclometalating 2-[3-(7-naphthalimidylfluoren-2′-yl)phenyl]pyridine ligands were synthesized and their photophysics and reverse saturable absorption were systematically investigated.